

Rheological Signature of Frictional Interactions in Shear Thickening Suspensions

John R. Royer,^{1,2} Daniel L. Blair,³ and Steven D. Hudson¹

¹*Materials Science and Engineering Division, National Institute of Standards and Technology, Gaithersburg, Maryland 20899, USA*

²*Institute for Bioscience and Biotechnology Research (IBBR), University of Maryland, Rockville, Maryland 20850, USA*

³*Department of Physics and Institute for Soft Matter Synthesis and Metrology, Georgetown University, Washington, D.C. 20057, USA*

(Received 13 November 2015; revised manuscript received 1 March 2016; published 5 May 2016)

Colloidal shear thickening presents a significant challenge because the macroscopic rheology becomes increasingly controlled by the microscopic details of short ranged particle interactions in the shear thickening regime. Our measurements here of the first normal stress difference over a wide range of particle volume fractions elucidate the relative contributions from hydrodynamic lubrication and frictional contact forces, which have been debated. At moderate volume fractions we find $N_1 < 0$, consistent with hydrodynamic models; however, at higher volume fractions and shear stresses these models break down and we instead observe dilation ($N_1 > 0$), indicating frictional contact networks. Remarkably, there is no signature of this transition in the viscosity; instead, this change in the sign of N_1 occurs while the shear thickening remains continuous. These results suggest a scenario where shear thickening is driven primarily by the formation of frictional contacts, with hydrodynamic forces playing a supporting role at lower concentrations. Motivated by this picture, we introduce a simple model that combines these frictional and hydrodynamic contributions and accurately fits the measured viscosity over a wide range of particle volume fractions and shear stress.

DOI: 10.1103/PhysRevLett.116.188301

There is mounting evidence from recent experiments [1,2] and simulations [3] suggesting that contact friction plays a dominant role in colloidal shear thickening; however, this assertion is controversial because of contrary evidence. While friction-based models and simulations capture the viscosity increase observed in experiments, other experimental signatures, particularly the stress anisotropy, are at odds with expectations for frictional interactions [4].

Shear thickening, where a suspension's viscosity $\eta = \sigma/\dot{\gamma}$ increases with increasing shear stress σ (or shear rate $\dot{\gamma}$), is important in a wide array of industrial processes and applications, either something to be avoided or a desired, engineered property [5–7]. Shear thickening is observed in both granular suspensions, where the particle diameter d is generally $d \gtrsim 10 \mu\text{m}$, and colloidal suspensions, where $d \lesssim 10 \mu\text{m}$. In granular suspensions, the evidence that friction drives shear thickening is well established [8–16], but in colloidal suspensions shear thickening is instead commonly attributed to diverging hydrodynamic lubrication forces, which lock particles together in correlated “hydroclusters” [17–21].

A key difference between friction and lubrication forces lies in the stress anisotropy generated by these two types of interactions. This difference is captured by the first normal stress difference $N_1 \equiv \sigma_{xx} - \sigma_{zz}$, where σ_{ij} is the stress tensor for a shear flow in the x direction with a gradient along z . Simulations based on hydrodynamic interactions show that shear-induced distortions of the suspension microstructure and short ranged lubrication forces drive $N_1 < 0$ [7,18,19,22]. Including repulsive interactions or elastic

particle deformations to these hydrodynamic models does not change the sign of N_1 [23–25], and N_1 is predicted to become increasingly negative as the particle concentration increases. In contrast, dilatancy ($N_1 > 0$) is a well-known feature of dense, frictional granular materials [9,26], reflecting the anisotropic nature of the force chain network [27].

While proposed friction-based models for shear thickening do not make explicit predictions for N_1 , at sufficiently high volume fractions one expects frictional contact networks to lead to dilation ($N_1 > 0$), as in the granular case. Only a handful of experiments measure N_1 in shear thickening colloids, though most report $N_1 < 0$ [4,28–30], consistent with lubrication forces; the lone exception is a study using roughened particles [31]. Recent experimental evidence for friction-driven colloidal shear thickening focuses on the viscosity alone, either comparing viscosity profiles to friction-based models [1] or using shear-reversal techniques to separate contributions from hydrodynamic and contact forces [2]; and thus these experiments do not address this discrepancy in the sign of N_1 .

In this Letter we address this disagreement between friction-based models and experiments. Detailing the behavior of both the viscosity $\eta(\sigma, \phi)$ and $N_1(\sigma, \phi)$ over a wide range of shear stresses and volume fractions in colloidal silica spheres exhibiting continuous shear thickening, we show that negative contributions to N_1 from lubrication forces can mask positive frictional contributions at moderate volume fractions; but at sufficiently high volume fractions and stresses, frictional interactions become dominant and N_1 transitions from negative to

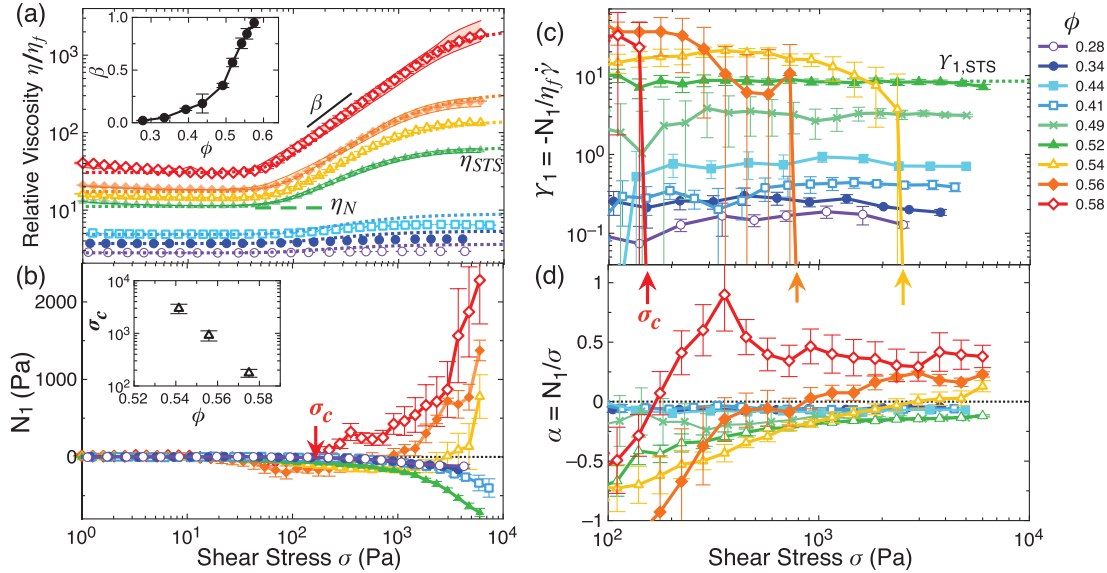


FIG. 1. Transition to dilation in shear thickening suspensions. (a) Relative viscosity $\eta_r(\sigma, \phi)$. Dotted lines: fits to Eq. (2) Inset: shear thickening exponent $\beta(\phi)$. (b) First normal stress difference $N_1(\sigma, \phi)$. Inset: crossover stress $\sigma_c(\phi)$ where N_1 crosses zero. (c) First normal stress difference coefficient $\Upsilon_1 \equiv -N_1/\eta_f\dot{\gamma}$. See Supplemental Material [33] for the $N_1 < 0$ results on an expanded scale [33]. (d) Stress ratio $\alpha = N_1/\sigma$. Error bars reflect the standard deviation from multiple up and down stress sweeps. Stress sweeps are conducted at several fixed temperatures: $T = 1, 10, 21$, and 35°C . Shaded regions in (a) show the range of η_r from $T = 1^\circ\text{C}$ (upper bound) to $T = 21^\circ\text{C}$ (lower bound) for $\phi \geq 0.52$; all other quantities are independent of T .

positive. This highlights the need to include both lubrication and friction to fully describe shear thickening at moderate volume fractions, suggesting possible modifications to purely friction-based models for shear thickening.

Here, we work with unmodified $d = 1.54 \mu\text{m}$ silica spheres (Bang Laboratories, Inc. [32]) suspended in a glycerol-water mixture (92% glycerol mass fraction). A small amount of salt is added to screen electrostatic interactions ($[\text{NaCl}] = 0.001 \text{ mole/L}$), so that the Debye screening length $\kappa^{-1} = 7 \text{ nm}$ is small compared to the particle size. We prepare samples with volume fractions $0.28 \leq \phi \leq 0.58$ from a concentrated stock suspension with $\phi_{\text{stk}} = 0.58$, which we determine from confocal imaging and particle locating in samples that have been index matched and diluted by a known ratio. Our relative uncertainty in ϕ due to uncertainty in d and particle locating errors is approximately 3%, e.g., $\phi_{\text{stk}} = 0.58 \pm 0.02$.

Rheology is performed under steady shear using an Anton-Paar MCR302 with a $R = 12.5 \text{ mm}$ radius cone-plate tool. In this geometry, N_1 can be measured from the axial force $N_1 = 2F_z/\pi R^2$. In order to access large shear stresses at all volume fractions over a limited range of shear rates, we perform stress sweeps at fixed temperatures between $T = 1^\circ\text{C}$ and $T = 35^\circ\text{C}$ to adjust the viscosity of the suspending fluid between $\eta_f = 1.7 \text{ Pa s}$ and $\eta_f = 0.107 \text{ Pa s}$. For $\phi \leq 0.52$, changing η_f has no impact on either the relative viscosity $\eta_r(\sigma) = \eta(\sigma)/\eta_f$ or $N_1(\sigma)$, and thus on the onset stress for shear thickening. At higher ϕ there is a slight increase in the shear thickening with

increasing η_f , though this variation is small compared to the variation between samples at different ϕ . At all ϕ both $\eta_r(\sigma)$ and $N_1(\sigma)$ are reversible, with no observable hysteresis in repeated up and down stress sweeps. Similarly, we do not observe time dependence at fixed σ , indicating that the flow curves in Fig. 1 reflect steady-state suspension properties. See Supplemental Material for additional details [33].

The relative viscosity $\eta_r(\sigma)$ [Fig. 1(a)] exhibits features characteristic of typical shear thickening colloidal suspensions [5,7]. At low σ there is mild shear thinning, followed by a plateau at a value $\eta_N(\phi)$, which we identify as the high-shear Newtonian plateau (see Supplemental Material [33]). As the stress is further increased, the viscosity begins to increase and then plateaus at a higher value $\eta_{\text{STS}}(\phi)$ i.e., the viscosity of the shear thickened state. The Newtonian plateau viscosity increases with volume fraction as $\eta_N(\phi) = (1 - \phi/\phi_0)^{-2}$ with $\phi_0 = 0.711 \pm 0.007$ [Fig. 2(a)], in good agreement with previous measurements of the high-shear viscosity in hard-sphere colloids [7,47]. We can fit the shear thickened plateau viscosity to the same form $\eta_{\text{STS}}(\phi) = (1 - \phi/\phi_m)^{-2}$ yielding $\phi_m = 0.592 \pm 0.006$. Distinct, diverging branches for the Newtonian and shear thickened viscosity plateaus are observed in other systems, though our measured ϕ_m is slightly larger than values reported in previous studies [1,30]. Though both η_N and η_{STS} increase with ϕ , the shear thickening onset stress is independent of ϕ , again consistent with previous experiments [1,30,48,49].

To characterize the steepness of the shear thickening, we fit the viscosity increase to $\eta_r \propto \sigma^\beta$. The onset of

discontinuous shear thickening (DST) is defined by $\beta = 1$, which implies a steady viscosity increase at a fixed shear rate, and $\beta < 1$ corresponds to continuous shear thickening. In our suspensions β increases monotonically with ϕ up to $\beta = 0.95 \pm 0.05$ at $\phi = 0.58$, approaching the DST onset.

While the transition to DST occurs at approximately $\phi = 0.58$, $N_1(\sigma, \phi)$ reveals a transition elaborated below that is not evident in η_r [Fig. 1(b)]. For $\phi \leq 0.52$, $N_1 \approx 0$ for $\sigma \lesssim 100$ Pa, then drops below zero and becomes increasingly negative as σ is increased. The decrease in N_1 becomes more pronounced as ϕ is increased up to $\phi = 0.52$. At higher volume fractions, $N_1(\sigma)$ initially decreases below zero as before, but as σ increases further $N_1(\sigma)$ reverses direction, crosses zero at a shear stress σ_c , and becomes positive.

Simulations based on lubrication hydrodynamics predict $N_1 < 0$ and that N_1 should scale linearly with $\dot{\gamma}$ in the high-shear limit [19,50], so that the dimensionless first normal stress coefficient $\Upsilon_1 \equiv -N_1/\eta_f \dot{\gamma}$ approaches a stress-independent constant. Below $\phi = 0.52$, where N_1 remains negative, we find that Υ_1 is indeed stress independent above $\sigma \approx 100$ Pa, while below this stress we cannot resolve N_1 [Fig. 1(c)]. The average value $\Upsilon_{1,\text{STS}}(\phi)$ increases monotonically with ϕ . An empirical relation

$$\Upsilon_{1,\text{STS}}(\phi) = K_1 \left(\frac{\phi}{\phi_{\text{max}}} \right)^2 \left(1 - \frac{\phi}{\phi_{\text{max}}} \right)^{-2}, \quad (1)$$

initially proposed to capture simulation results [50], was shown to fit experimental results for $\phi \leq 0.52$ with $K_1 = 0.177 \pm 0.022$ and $\phi_{\text{max}} = \phi_m$ obtained from $\eta_{\text{STS}}(\phi)$ [30]. Our results for $\phi \leq 0.52$ can be fit using this same expression [Fig. 2(b)], with a nearly identical coefficient $K_1 = 0.14 \pm 0.01$.

At higher volume fractions $\Upsilon_1(\sigma)$ is no longer stress independent, but instead changes sign as the suspensions become dilatant. As ϕ increases, the crossover stress σ_c decreases, in contrast to the shear thickening onset stress that remains independent of ϕ . Below σ_c , we can identify a plateau in Υ_1 over a limited range of σ . This initial plateau follows Eq. (1) up to $\phi = 0.56$, even though $\Upsilon_1(\sigma)$ eventually drops below zero. At $\phi = 0.58$, the stress ratio $\alpha = N_1/\sigma$ is approximately constant in the high-stress limit [Fig. 1(d)], consistent with a simple geometric model for force chains [27].

To characterize the stress ratio in the high-shear limit, we define $\alpha_{\text{STS}}(\phi)$, taking the average over $\sigma \geq 2500$ Pa. Below $\phi = 0.52$, where N_1 remains negative, α_{STS} slightly decreases with increasing ϕ . Noting that Υ_1 can be rewritten as $\Upsilon_1 = -(N_1/\sigma)\eta_r = -\alpha\eta_r$, we see that the singular term in Eq. (1) can be solely ascribed to the viscosity divergence. Thus, as long as the stress ratio α remains bounded, fits to Eq. (1) are guaranteed to give the same $\phi_{\text{max}} = \phi_m$ where η_{STS} diverges, but do not imply that N_1 and η_r are necessarily linked. If lubrication forces drive

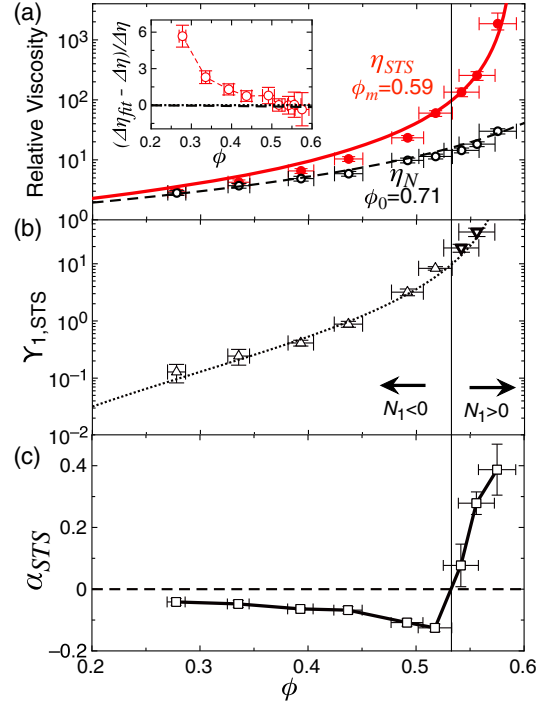


FIG. 2. Limiting behavior of η_r and N_1 . (a) Newtonian viscosity η_N (open circles) and the shear thickened plateau η_{STS} (solid circles). Lines show fits $\eta_N = (1 - \phi/\phi_0)^{-2}$ (dashed line) and $\eta_{\text{STS}} = (1 - \phi/\phi_m)^{-2}$ (solid line). Inset: difference between measured $\Delta\eta \equiv \eta_{\text{STS}} - \eta_N$ and fitted expressions. (b) $\Upsilon_{1,\text{STS}}(\phi)$. Triangles: values where $N_1 < 0$. Upside-down triangles: plateau values below σ_c . Dotted line: fit to Eq. (1). (c) Stress ratio α_{STS} . Uncertainties in ϕ are 3% as noted in the text. Uncertainties in η_{STS} , $\Upsilon_{1,\text{STS}}$, and α_{STS} reflect the standard deviation from averaging over $\sigma > 2500$ Pa.

the rise in η_{STS} , N_1 should become increasingly negative as $\phi \rightarrow \phi_m$. Instead, N_1 changes dramatically and becomes positive prior to reaching ϕ_m , revealing a lack of coupling between the viscosity and N_1 .

Positive values of N_1 suggest that frictional forces are present and become dominant as $\phi \rightarrow \phi_m$. Motivated by this, we fit $\eta_r(\sigma, \phi)$ using a recently proposed friction-based model [1,15]. The model assumes $\eta_r(\phi)$ is controlled by two distinct divergences, one at $\phi = \phi_0$ for frictionless contacts and a second at a friction-dependent $\phi_m < \phi_0$, giving the two branches η_{STS} and η_N shown in Fig. 2(a). The full flow curves are given by

$$\eta_r(\sigma, \phi) = \left(1 - \frac{\phi}{\phi_c(\sigma)} \right)^{-2}, \quad (2)$$

where $\phi_c(\sigma) = f\phi_m + (1 - f)\phi_0$ interpolates between the two maximum volume fractions and $f \in [0, 1]$ represents the fraction of frictional contacts. In this model, contacts become frictional when the compressive force between neighbors exceeds a repulsive stabilizing force F_{rep} . While the precise form of $f = f(\sigma, \phi)$ depends on the microstructure and the local contact force distribution, we first

adopt a simple ansatz $f(\sigma) = e^{-\sigma^*/\sigma}$. This form is also used in [1], which the authors motivate by assuming an exponential contact force distribution and counting the fraction of local forces above F_{rep} , which sets the threshold stress $\sigma^* \propto F_{\text{rep}}/d^2$.

This friction-based model fits our results at high volume fractions, where we find $N_1 > 0$, exceptionally well [Fig. 1(a)]. Here, we hold $\phi_m = 0.592$ fixed, but leave both σ^* and ϕ_0 as adjustable parameters. Allowing ϕ_0 to vary accounts for scatter in $\eta_N(\phi)$, though the fitted values agree with $\phi_0 = 0.71$ within uncertainty. At lower volume fractions, where we find $N_1 < 0$, there is neither change in the shear thickening onset nor any qualitative change in the viscosity profile $\eta_r(\sigma)$, suggesting this same model can be applied. Indeed, Fig. 1 shows that even though N_1 is strongly negative for $\phi = 0.52$, dropping to as low as -700 Pa, this friction-based model still captures the shear thickening.

The model fits begin to overshoot the amount of shear thickening below $\phi \lesssim 0.5$ [Fig. 3(a)]. Though the absolute magnitude of this overshoot is small, this discrepancy can be seen in the limiting viscosities, where the relative difference between measured and fitted values for $\Delta\eta \equiv \eta_{\text{STS}} - \eta_N$ increases with decreasing ϕ [Fig. 2(a)]. We attribute this disagreement to our simple ansatz for $f(\sigma)$, where $f \rightarrow 1$ for $\sigma \gg \sigma^*$, independent of ϕ . While we might expect this close to ϕ_m , in dilute suspensions we expect the flow to be dominated by momentary collisions as opposed to enduring contacts. If we instead take

$f(\sigma, \phi) = f_{\text{max}}(\phi)e^{-\sigma^*/\sigma}$ with $0 \leq f_{\text{max}} \leq 1$, we can fit $\eta(\sigma, \phi)$ over our full range of ϕ . We find that the *ad hoc* parameter $f_{\text{max}} \approx 1$ for $\phi \gtrsim 0.5$, but below this point f_{max} monotonically decreases with decreasing ϕ [Fig. 3(b)].

To understand the regime where $f_{\text{max}} < 1$, we posit that the formation of enduring frictional contacts requires not only temporary local stresses exceeding σ^* , but also a confining force to maintain these contacts. At moderate ϕ this many-body confinement could be provided by hydrodynamic lubrication forces, reminiscent of the hydrocluster model. In this speculative scenario, shear thickening is driven by the formation of frictional contacts within hydroclusterlike structures, though the fraction of frictional contacts is limited by the size of these clusters so that $f_{\text{max}} < 1$. Since frictional contacts are confined within these finite clusters, there are no system-spanning force chains and the normal stress difference is dominated by lubrication forces, giving $N_1 < 0$. At some $\phi_{\text{perc}} < \phi_m$ these clusters span the system so that $f_{\text{max}} \approx 1$ and frictional contact networks percolate throughout the system, driving the transition to $N_1 > 0$.

The scenario proposed here bridges competing friction-driven and lubrication-driven explanations for colloidal shear thickening. At moderate concentrations, hydrodynamic forces distort the microstructure and bring particles together, consistent with previous experiments where hydroclusterlike structures have been observed [21] and negative values of N_1 directly linked to hydrodynamic stresses [4]. However, the viscosity increase is ultimately driven by the formation of frictional contacts within these clusters, consistent with recent experimental evidence for friction-driven shear thickening [1,2]. This scenario differs from proposed mechanisms for the onset of DST in granular suspensions [8,9]. Instead of dilation driving shear thickening, both dilation and shear thickening are separate consequences of frictional interactions. Dilation requires system-spanning frictional contacts and hence high volume fractions, while shear thickening can result from non-system-spanning frictional contacts and hence occurs over a wider range of volume fractions.

The transition in the sign of N_1 observed here is qualitatively similar to results with roughened silica spheres [31], where the onset of dilation at $\phi = 0.43$ also precedes the transition to DST at $\phi = 0.455$. Both transitions occur at lower volume fractions, which we would expect as enhanced roughness should increase the particle friction and decrease ϕ_m ; this may also explain the difference between values in previous experiments [1,30]. Recent simulations that include both lubrication and frictional interactions show a similar transition in the sign of N_1 , with $N_1 \lesssim 0$ at $\phi = 0.5$ and 0.53 , but $N_1 > 0$ at $\phi = 0.55$ [3]. Other simulations, which also include lubrication and friction but only explore moderate volume fractions $\phi \leq 0.45$, find that friction weakly increases N_1 but overall N_1 remains negative [51,52], again consistent with our

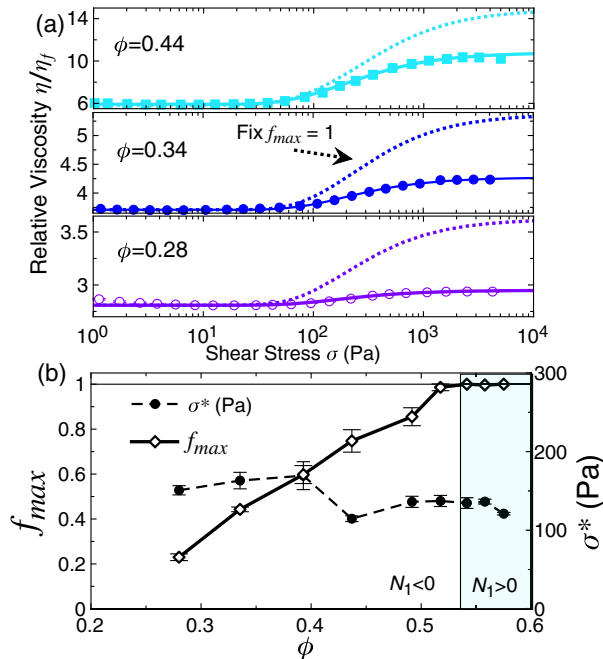


FIG. 3. Model comparison. (a) $\eta_r(\sigma)$ at selected ϕ , showing fits to Eq. (2) fixing $f_{\text{max}} = 1$ (dotted lines) and letting f_{max} vary (solid lines). (b) f_{max} and σ^* extracted from fits to Eq. (2). Uncertainties in σ^* and f_{max} reflect the standard uncertainty from these fits.

results. Normal stress differences have the potential to serve as a sensitive diagnostic of particle interactions, particularly the presence of frictional interactions. Our results highlight the need for additional studies to determine the effects of particle size, roughness, and other surface properties.

We thank J. Seppala and E. Del Gado for insightful discussions, and A. Forster for assistance with supplementary tests. D.L.B. acknowledges the support of Cooperative Agreement No. 70NANB15H229 from NIST, U.S. Department of Commerce, The John F. Templeton Foundation Grant No. 57392 and the National Science Foundation Grant No. DMR-0847490. This work is a contribution of NIST, an agency of the U.S. Government, and not subject to U.S. copyright.

-
- [1] B. M. Guy, M. Hermes, and W. C. K. Poon, *Phys. Rev. Lett.* **115**, 088304 (2015).
- [2] N. Y. C. Lin, B. M. Guy, M. Hermes, C. Ness, J. Sun, W. C. K. Poon, and I. Cohen, *Phys. Rev. Lett.* **115**, 228304 (2015).
- [3] R. Mari, R. Seto, J. F. Morris, and M. M. Denn, *Proc. Natl. Acad. Sci. U.S.A.* **112**, 15326 (2015).
- [4] A. K. Gurnon and N. J. Wagner, *J. Fluid Mech.* **769**, 242 (2015).
- [5] H. A. Barnes, *J. Rheol.* **33**, 329 (1989).
- [6] E. Brown and H. M. Jaeger, *Rep. Prog. Phys.* **77**, 046602 (2014).
- [7] J. Mewis and N. Wagner, *Colloidal Suspension Rheology* (Cambridge University Press, Cambridge, 2011).
- [8] A. Fall, N. Huang, F. Bertrand, G. Ovarlez, and D. Bonn, *Phys. Rev. Lett.* **100**, 018301 (2008).
- [9] E. Brown and H. M. Jaeger, *J. Rheol.* **56**, 875 (2012).
- [10] N. Fernandez, R. Mani, D. Rinaldi, D. Kadau, M. Mosquet, H. Lombois-Burger, J. Cayer-Barrioz, H. J. Herrmann, N. D. Spencer, and L. Isa, *Phys. Rev. Lett.* **111**, 108301 (2013).
- [11] C. Heussinger, *Phys. Rev. E* **88**, 050201 (2013).
- [12] R. Seto, R. Mari, J. F. Morris, and M. M. Denn, *Phys. Rev. Lett.* **111**, 218301 (2013).
- [13] Q. Xu, S. Majumdar, E. Brown, and H. M. Jaeger, *Europhys. Lett.* **107**, 68004 (2014).
- [14] R. Mari, R. Seto, J. F. Morris, and M. M. Denn, *J. Rheol.* **58**, 1693 (2014).
- [15] M. Wyart and M. E. Cates, *Phys. Rev. Lett.* **112**, 098302 (2014).
- [16] C. Ness and J. Sun, *Soft Matter* **12**, 914 (2016).
- [17] J. R. Melrose and R. C. Ball, *Europhys. Lett.* **32**, 535 (1995).
- [18] T. N. Phung, J. F. Brady, and G. Bossis, *J. Fluid Mech.* **313**, 181 (1996).
- [19] D. R. Foss and J. F. Brady, *J. Fluid Mech.* **407**, 167 (2000).
- [20] N. J. Wagner and J. F. Brady, *Phys. Today* **62**, 27 (2009).
- [21] X. Cheng, J. H. McCoy, J. N. Israelachvili, and I. Cohen, *Science* **333**, 1276 (2011).
- [22] J. Bergenholtz, J. F. Brady, and M. Vucic, *J. Fluid Mech.* **456**, 239 (2002).
- [23] J. R. Melrose and R. C. Ball, *J. Rheol.* **48**, 961 (2004).
- [24] J. R. Melrose and R. C. Ball, *J. Rheol.* **48**, 937 (2004).
- [25] S. Jamali, A. Boromand, N. Wagner, and J. Maia, *J. Rheol.* **59**, 1377 (2015).
- [26] O. Reynolds, *Philos. Mag.* **20**, 469 (1885).
- [27] M. E. Cates, J. P. Wittmer, J.-P. Bouchaud, and P. Claudin, *Phys. Rev. Lett.* **81**, 1841 (1998).
- [28] H. M. Laun, *J. Non-Newtonian Fluid Mech.* **54**, 87 (1994).
- [29] M. Lee, M. Alcoutlabi, J. J. Magda, C. Dibble, M. J. Solomon, X. Shi, and G. B. McKenna, *J. Rheol.* **50**, 293 (2006).
- [30] C. D. Cwalina and N. J. Wagner, *J. Rheol.* **58**, 949 (2014).
- [31] D. Lootens, H. van Damme, Y. Hémar, and P. Hébraud, *Phys. Rev. Lett.* **95**, 268302 (2005).
- [32] Certain instruments and materials are identified in this paper to adequately specify the experimental details. Such identification does not imply recommendation by the National Institute of Standards and Technology; nor does it imply that the materials are necessarily the best available for the purpose.
- [33] See Supplemental Material at <http://link.aps.org/supplemental/10.1103/PhysRevLett.116.188301>, which includes Refs. [34–46], for additional details concerning the dependence of η_r and N_1 on temperature, Péclet number and time, as well as a comparison between η_N and previous experiments.
- [34] W. H. Boersma, P. J. M. Baets, J. Laven, and H. N. Stein, *J. Rheol.* **35**, 1093 (1991).
- [35] C. G. de Kruif, E. M. F. van Iersel, A. Vrij, and W. B. Russel, *J. Chem. Phys.* **83**, 4717 (1985).
- [36] W. C. K. Poon, E. R. Weeks, and C. P. Royall, *Soft Matter* **8**, 21 (2012).
- [37] W. B. Russel, N. J. Wagner, and J. Mewis, *J. Rheol.* **57**, 1555 (2013).
- [38] Y. S. Papir and I. M. Krieger, *J. Colloid Interface Sci.* **34**, 126 (1970).
- [39] M. E. Woods and I. M. Krieger, *J. Colloid Interface Sci.* **34**, 91 (1970).
- [40] J. C. van der Werff and C. G. de Kruif, *J. Rheol.* **33**, 421 (1989).
- [41] I. E. Zarraga, D. A. Hill, and D. T. Leighton, *J. Rheol.* **44**, 185 (2000).
- [42] A. Singh and P. R. Nott, *J. Fluid Mech.* **490**, 293 (2003).
- [43] S.-C. Dai, E. Bertevas, F. Qi, and R. I. Tanner, *J. Rheol.* **57**, 493 (2013).
- [44] T. Dbouk, L. Lobry, and E. Lemaire, *J. Fluid Mech.* **715**, 239 (2013).
- [45] C. Gamonpilas, J. F. Morris, and M. M. Denn, *J. Rheol.* **60**, 289 (2016).
- [46] C. R. Schultheisz and S. D. Leigh, in *NIST Special Publication 260-143* (U.S. Department of Commerce, Technology Administration, NIST, Washington, D.C., 2001).
- [47] S.-E. Phan, W. B. Russel, Z. Cheng, J. Zhu, P. M. Chaikin, J. H. Dunsmuir, and R. H. Ottewill, *Phys. Rev. E* **54**, 6633 (1996).
- [48] B. J. Maranzano and N. J. Wagner, *J. Rheol.* **45**, 1205 (2001).
- [49] B. J. Maranzano and N. J. Wagner, *J. Chem. Phys.* **114**, 10514 (2001).
- [50] J. F. Morris and F. Boulay, *J. Rheol.* **43**, 1213 (1999).
- [51] A. Sierou and J. F. Brady, *J. Rheol.* **46**, 1031 (2002).
- [52] S. Gallier, E. Lemaire, F. Peters, and L. Lobry, *J. Fluid Mech.* **757**, 514 (2014).

Supplementary Material for ‘A rheological signature of frictional interactions in shear thickening suspensions’

John R. Royer, Daniel L. Blair, and Steven D. Hudson
(Dated: April 4, 2016)

I. TEMPERATURE DEPENDENCE

In the rheology presented here, stress-sweeps are conducted at selected temperatures between $T = 1\text{ }^\circ\text{C}$ and $T = 35\text{ }^\circ\text{C}$. This allows us to adjust the viscosity of the glycerol-based suspending fluid over an order of magnitude, from $\eta_f = 1.7\text{ Pa s}$ down to $\eta_f = 0.107\text{ Pa s}$. A temperature control hood and solvent trap minimize exposure to ambient air, helping maintain a uniform temperature ($\pm 0.01\text{ }^\circ\text{C}$) and preventing the suspension from either absorbing extra water or drying out at the edge. We use a $R = 12.5\text{ mm}$ radius cone-plate TruGap (TM) tool with a 1 degree cone angle and $0.052\text{ }\mu\text{m}$ truncation gap. The sample temperature is set by a peltier in the bottom plate, and additional peltiers in the temperature control hood maintain a uniform temperature around the sample. The TruGap system maintains a constant gap size as the temperature is varied. A constant shear stress $\sigma = 20\text{ Pa}$ is applied for 10 minutes prior to collecting data. There is a slight index mismatch between the fluid and particles, but index-matched samples exhibit nearly identical rheology. Adjusting η_f enabled access to a wide range of shear stresses over a limited range of shear rates at all volume fractions. At moderate volume fractions $\phi < 0.5$ we limited the maximum shear rate to $\dot{\gamma}_{max} = 1000\text{ s}^{-1}$ to avoid inertial contributions to the viscosity and normal stress difference. At higher volume fractions we further restricted $\dot{\gamma}_{max} = 200\text{ s}^{-1}$ to avoid flow instabilities (associated with granulation and edge fracture) that could eject the suspension from the tool geometry.

For $\phi \leq 0.52$, though the physical viscosity $\eta(\sigma, T)$ varies strongly with temperature, the relative viscosity $\eta_r(\sigma, T) = \eta(\sigma, T)/\eta_f(T)$ collapses onto a single curve, with no significant change in either the shear thickening onset stress or the plateau viscosity η_{STS} [Fig. 1(a)]. Likewise, the (unnormalized) first normal stress difference is temperature independent. At higher volume fractions N_1 remains independent of temperature, but there is a slight variation in $\eta_{STS}(\phi, T)$, with η_{STS} slightly larger at lower temperatures (higher η_f) [Fig. 1(b)]. We speculate that this variation in η_{STS} may reflect enhanced wall slip in the shear thickening regime at high volume fractions [1], but note this temperature dependence is rather weak for the range of temperatures explored in this work.

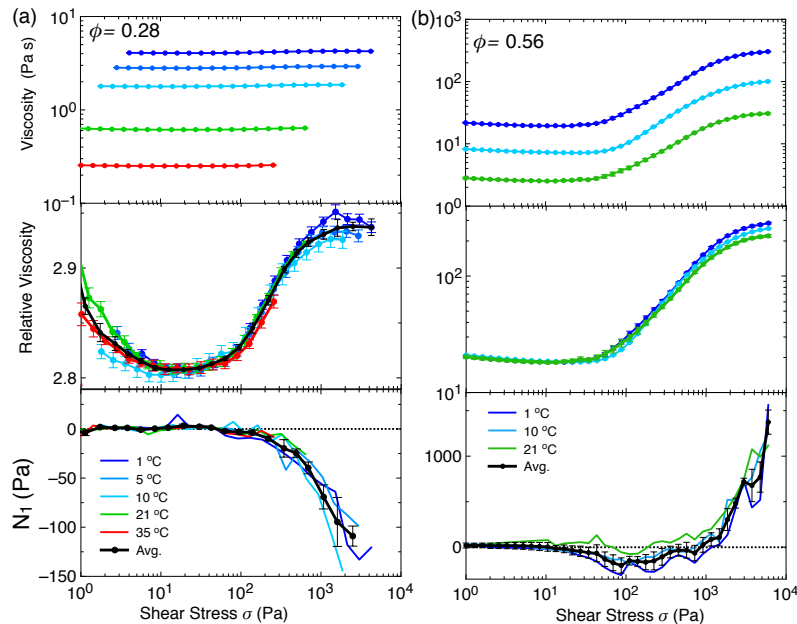


FIG. 1. Top to bottom: Viscosity, relative viscosity and first normal stress difference at various temperatures for (a) $\phi = 0.29$ and (b) $\phi = 0.56$.

II. TIME DEPENDANCE

The flow curves presented here were obtained with a variable, software controlled time step, nominally taking 15 s per data point. To check for any time dependence in the the measured $\eta_r(\sigma, \phi)$ or $N_1(\sigma, \phi)$ we conducted tests measuring $\eta_r(t)$ and $N_1(t)$ for up to 500 s at selected values of the shear stress, covering the Newtonian plateau, the shear thickening transition and the shear thickened plateau [Fig. 2]. The time averaged steady-state values obtained in these time dependent tests agree very well with the values obtain in the stress sweeps, demonstrating that the rheology presented here represents true steady properties, even in dilatant samples where $N_1 > 0$.

In Fig. 3 we examine the time dependence of $\eta_r(t)$ and $N_1(t)$ in more detail. In all cases, the measured values of $\eta_r(t)$ and $N_1(t)$ stay very close to the average values measured in the stress sweeps, with negligible drift. The fluctuations in both $\eta_r(t)$ and $N_1(t)$ are slightly more pronounced at in the regime where $N_1 > 0$, ($\sigma = 5000$ Pa, $\phi = 0.56$), but not nearly as a severe as the stress and viscosity fluctuations that accompanied dilatant flow in roughened glass particles close to the DST transitions [2].

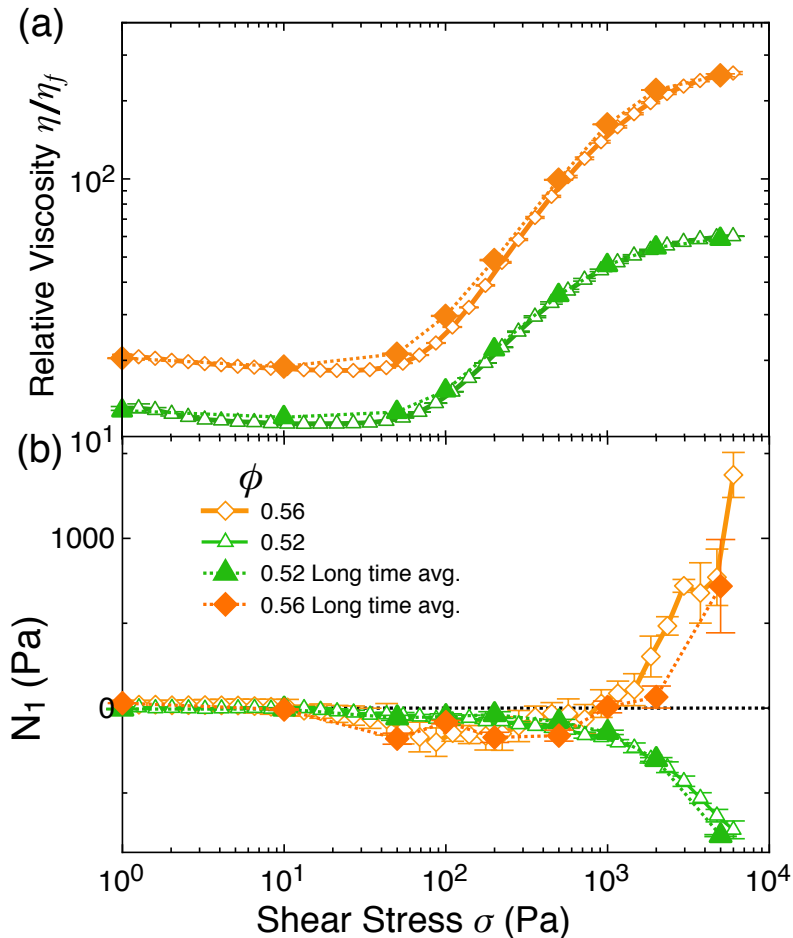


FIG. 2. Comparing the rheology measured in stress-sweep experiments with steady-state behavior. Large solid symbols: steady-state time-averaged values for $\bar{\eta}_r$ and \bar{N}_1 holding a constant stress for 500 s.

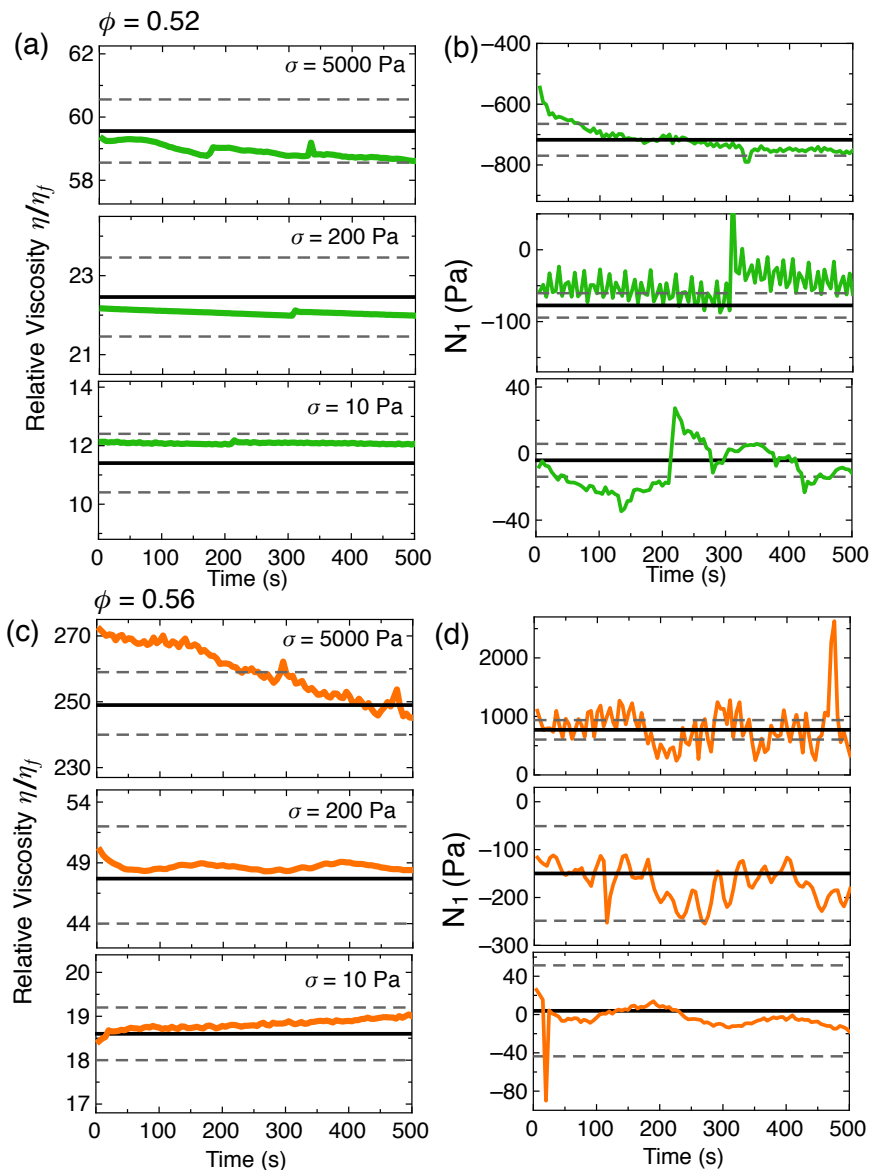


FIG. 3. Time dependence of $\eta_r(t)$ and $N_1(t)$ at $\phi = 0.52$ [(a) and (b)] and $\phi = 0.56$ [(c) and (d)]. Time-Dependent measurements were performed through an increasing sweep through selected values the shear stress (corresponding to the large solid symbols in Supplemental Fig. 2), holding the stress fixed at each value for 500 s and measuring $\eta(t)$ and $N_1(t)$ with a sampling time of 5 s per data point. The time $t = 0$ corresponds to the shear stress was increased from the previous value to the current value. Solid lines show average values from the stress-sweep runs. Dashed lines show the standard deviation from multiple up-down sweeps. From top to bottom in each section $\sigma = 10$ Pa, $\sigma = 200$ Pa, $\sigma = 5000$ Pa.

III. BROWNIAN STRESSES

In the absence of any external forces, the stresses in a colloidal suspension in equilibrium are isotropic, so that $N_1 = 0$. At low shear rates, where the shear is slow compared to the timescale for Brownian motion so that the Péclet number $Pe = 3\pi\eta_f d^3\dot{\gamma}/4k_B T$ is small but non-zero ($0 < Pe \lesssim 1$), Brownian stresses generate small, positive contributions to N_1 . [3–5] However, the hydrodynamic contribution to N_1 is always negative, and at higher shear rates where $Pe \gg 1$ the Brownian contribution is negligible and the hydrodynamic forces drive $N_1 < 0$, as discussed in the main text. Similarly, changing Brownian and hydrodynamic contributions to the shear stress drive shear thinning behavior, where the viscosity decreases with increasing Pe before reaching the a Newtonian plateau η_N at high Pe . [4, 6]

In the experiments here we work at a fixed range of shear stress $1 \text{ Pa} \leq \sigma \leq 6000 \text{ Pa}$. Using $\sigma = \eta\dot{\gamma} = \eta_f\eta_r\dot{\gamma}$, the

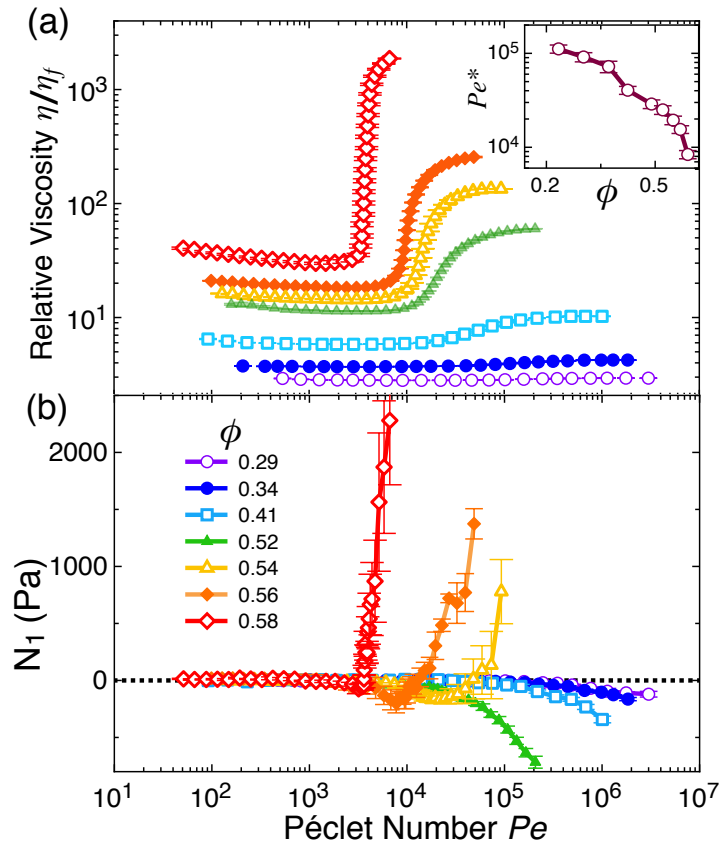


FIG. 4. Relative viscosity (a) and first normal stress difference (b) plotted against Péclet number Pe (same data as Fig. 1 of the main paper). Inset shows $Pe^*(\phi)$ corresponding to the shear thickening onset.

Péclet number can be written as

$$Pe = \frac{3\pi d^3 \sigma}{4k_B T \eta_r}. \quad (1)$$

Note that for a fixed range σ , the range of Pe varies depending on the relative viscosity of the suspension. In Fig. 4 we re-plot the data from Fig. 1 of the main text against Pe to illustrate the range of Pe probed in this work. At $\phi = 0.58$ our lowest $Pe \approx 50$ and some shear thinning is still evident. At lower volume fractions the range of Pe is higher, Brownian stresses are weaker and shear thinning is difficult to discern. The shear thickening onset occurs at high Péclet numbers Pe^* that vary strongly with ϕ , from $Pe^* \approx 10^4$ at $\phi = 0.58$ up to $Pe^* \gtrsim 10^5$ at $\phi = 0.28$. In contrast, the onset stress $\sigma^* \approx 140$ Pa is roughly constant. Although our silica spheres fall within the typical colloidal size range, the shear thickening we observe occurs well into the high-shear regime and consequently Pe is not a useful metric. Likewise, positive contributions to N_1 from Brownian stresses are negligible.

IV. NEWTONIAN (HIGH-SHEAR) VISCOSITY η_N

Given the high Péclet numbers probed here, we can identify the Newtonian viscosity η_N reached prior to the shear thickening onset with the the high-shear Newtonian plateau, sometimes denoted η_∞ even though shear thickening occurs at even higher shear rates. Our measurements for $\eta_N(\phi)$ are somewhat lower than values reported in a recent work exploring shear thickening with sterically stabilized PMMA spheres [7] and our fitted value of $\phi_0 = 0.71$ differs from their value $\phi_0 \approx 0.64$. They also measure a lower value of $\phi_m \approx 0.56$, while another recent study using sterically stabilized silica particles found $\phi_m \approx 0.54$, though they did not report a value of ϕ_0 [8]. We note that our results agree well with values for the high-shear viscosity for near-hard-sphere colloids reported by numerous other groups [Fig. 5]. This higher value of $\phi_0 = 0.71$ exceeds random close packing $\phi_{RCP} \approx 0.64$ for mono-disperse hard spheres,

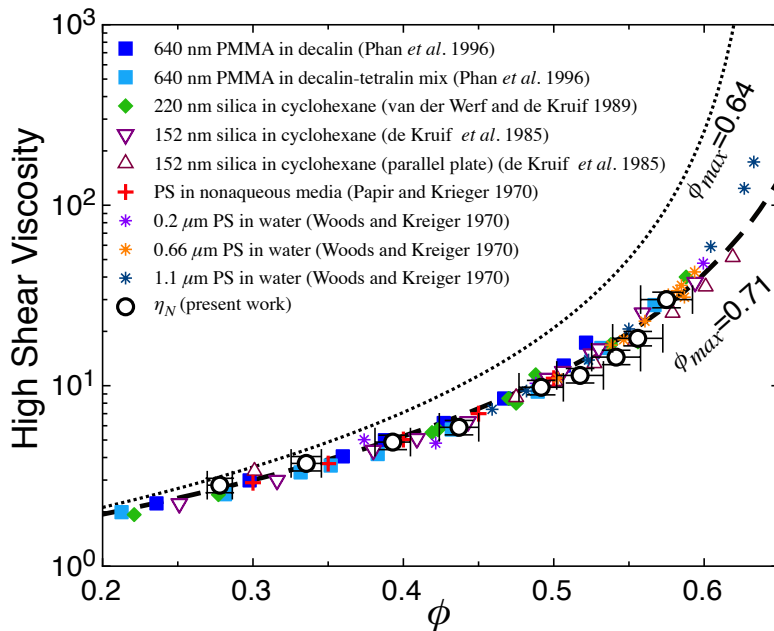


FIG. 5. High shear viscosity. Adapted from refs. [11, 12], and containing data from refs. [9, 13–15], as well as the $\eta_N(\phi)$ measured in this work. Dashed line shows $\eta_r = (1 - \phi/\phi_{max})^{-2}$ with $\phi_{max} = 0.71$. Dotted line shows $\phi_{max} = 0.64$.

and is sometimes attributed to flow-induced ordering in the high-shear limit [9]. It is possible this discrepancy can be attributed to differences in the particle size distributions in the different colloidal samples or perhaps to other details in the particle interactions. In the works reporting lower values of ϕ_0 the shear thinning and shear thickening regimes are not as well separated as they are in this work, so it is also possible they do not reach the same limiting hard sphere high-shear plateau. However, uncertainty and discrepancies between different methods of measuring the volume fraction ϕ are a common feature in colloidal experiments [10]. We note that the conclusions in these works do not depend on the precise values of either ϕ_0 or ϕ_m , only that $\phi_m < \phi_0$ which would not change with an overall rescaling of ϕ .

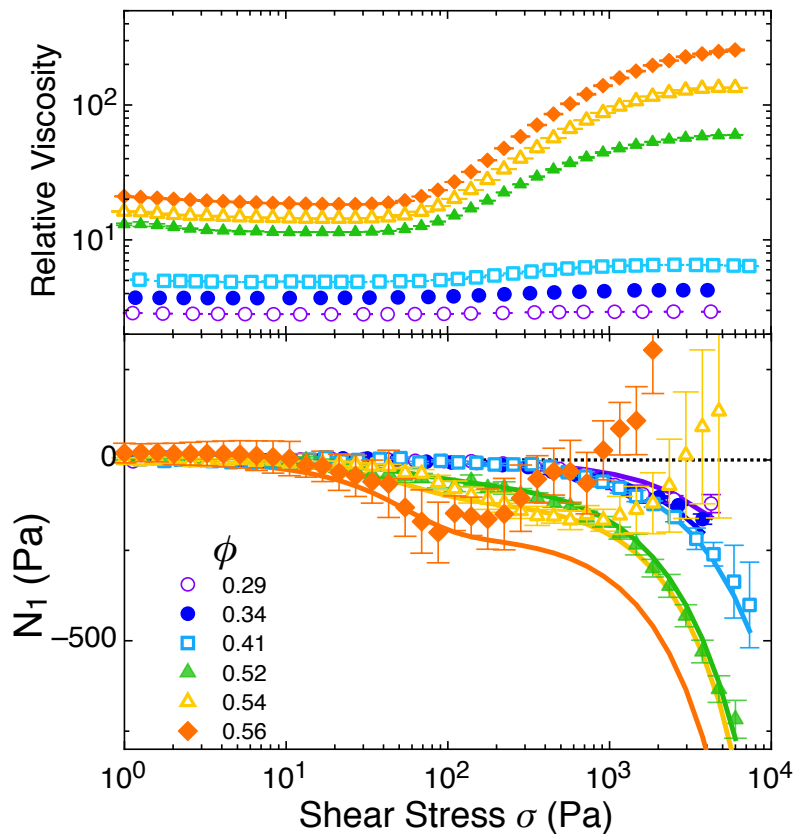


FIG. 6. Detailed view of the $N_1 < 0$ regime. Data for η_r and N_1 from Fig. 1 of the main paper up to $\phi = 0.56$, re-plotted to highlight the $N_1 < 0$ regime. Solid lines show results for the hydrodynamic scaling law $N_1 = -\mathcal{Y}_1(\phi)\eta_f\dot{\gamma}$, with $\mathcal{Y}_1(\phi)$ given by Eq. 1 of the main text.

V. EXPANDED SCALE FOR $N_1 < 0$ RESULTS

To better highlight the transition from $N_1 < 0$ to $N_1 > 0$ at higher volume fractions and shear stresses, we re-plot data from Fig. 1 of the main text focusing on the $N_1 < 0$ regime. This makes the initial decrease in N_1 below zero at $\phi = 0.54$ and $\phi = 0.56$ more readily apparent.

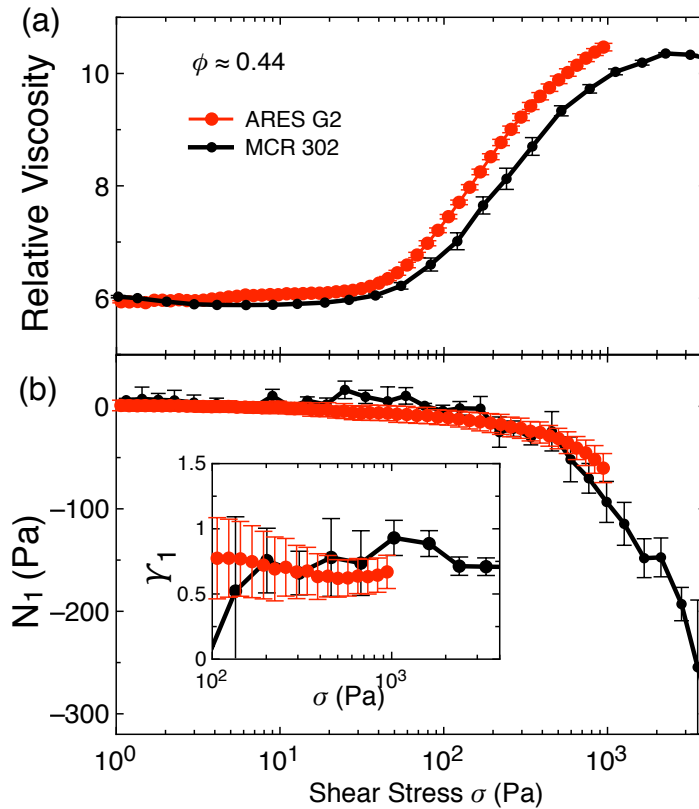


FIG. 7. Measuring viscosity and N_1 with 2 different rheometers. Relative viscosity (a) and first normal stress difference (b) for $\phi = 0.44$ measured on the MCR 302 (Anton Paar) used for the bulk of this work and on an Ares G2 strain controlled rheometer (TA instruments) [16]. In both cases the temperature was fixed at $T = 10^\circ \text{C}$ and a $R = 12.5$ mm cone-plate tool was used. On the MCR 302 the cone angle was $\alpha = 1.0^\circ$ while on the Ares G2 this angle was larger $\alpha = 5.8^\circ$. The inset in (b) shows the dimensionless first normal stress difference coefficient $\gamma_1 = -N_1/\eta_f \dot{\gamma}$.

VI. ACCURACY AND ROBUSTNESS OF N_1 MEASUREMENTS

As we discuss in the main text, prior measurements of N_1 in colloidal suspensions generally report $N_1 < 0$, [8, 17–19] with the noted exception of roughened spheres [2]. In suspensions of larger, non-Brownian suspensions ($d \gtrsim 10 \mu\text{m}$) experimental measurements of N_1 are less consistent, with some groups [20–22] finding $N_1 < 0$ but others [23, 24] finding $N_1 > 0$ for similar ranges of ϕ . We note that N_1 measurements can be more challenging in suspensions of larger particles because finite size effects become more pronounced in a standard cone-plate geometry. In many of these experimental studies either modifications to the cone-plate geometry or local pressure sensors were used to when measuring N_1 , which may influence the results. It is also possible that the discrepancies arise from differences in the different fluid-particle systems. In the references highlighted here, shear thickening is not observed and instead many of these non-Brownian suspensions exhibit mild shear thinning, making it difficult to compare the measurements of N_1 to our results. Given the spread of results observed in previous experiments, we performed additional test to verify the robustness of our N_1 measurements.

In Figure 7 we compare $\eta_r(\sigma)$ and $N_1(\sigma)$ measured in a suspension with $\phi = 0.44$ using our MCR 302 rheometer against measurements on an Ares G2 (TA instruments). Experiments on the Ares G2 we carried out with a $R = 12.5$ mm cone-plate tool with a wider cone angle, $\alpha = 5.8^\circ$ versus $\alpha = 1.0^\circ$ on the MCR 302. This geometry required roughly five times as much material for a single experiment, limiting work on this system to a single sample at $\phi = 0.44$. Despite the differences in the tool geometries available for the two different systems, both $\eta_r(\sigma)$ and $N_1(\sigma)$ are in excellent across the two systems.

To ensure robust measurements of N_1 in dilatant materials, we performed measurements on the MCR 302 [16] using a NIST rheology standard SRM-2490, a dilatant polymer solution (Polyisobutylene dissolved in 2,6,10,14-Tetramethylpentadecane). These measurements were carried out under identical conditions as our original measurements for shear rates ranging from $\dot{\gamma} = 0.1 \text{ s}^{-1}$ to $\dot{\gamma} = 100 \text{ s}^{-1}$ at $T = 25^\circ \text{C}$ and $T = 0^\circ \text{C}$. Under these conditions, we closely match the range of shear rates, temperature, shear stress probed in our experiments. Our results agree

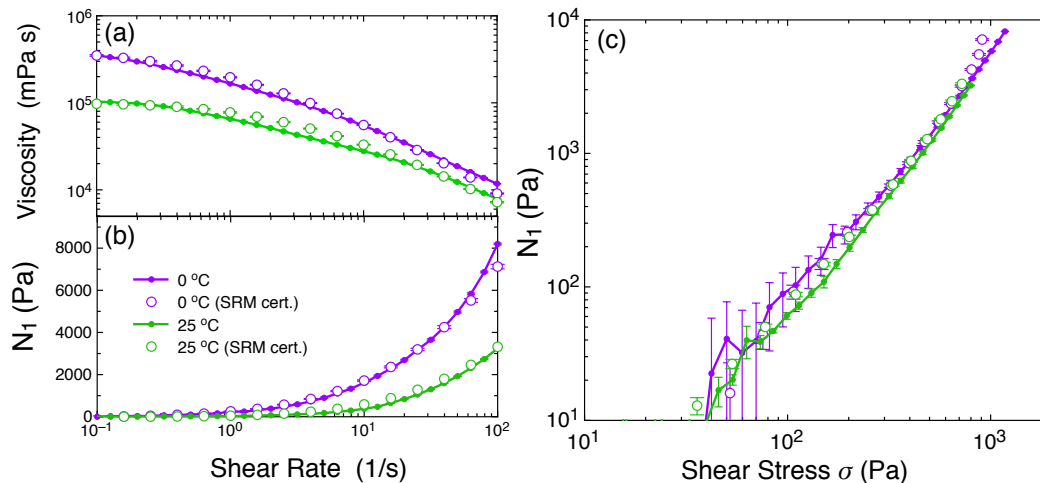


FIG. 8. Measuring viscosity and N_1 for NIST rheology reference material SRM 2490. Closed symbols: Data taken on our MRC 302 rheometer, using the same tool geometry and measurement procedure used in the suspension rheology measurements. Open symbols: Published reference data [25].

exceptionally well with the published reference values [Fig. 8], demonstrating the ability to measure accurately normal stress differences in dilatant materials.

-
- [1] W. H. Boersma, P. J. M. Baets, J. Laven, and H. N. Stein, *J. Rheol.* **35**, 1093 (1991).
 [2] D. Lootens, H. van Damme, Y. Hémar, and P. Hébraud, *Phys. Rev. Lett.* **95**, 268302 (2005).
 [3] T. N. Phung, J. F. Brady, and G. Bossis, *J. Fluid Mech.* **313**, 181 (1996).
 [4] D. R. Foss and J. F. Brady, *J. Fluid Mech.* **407**, 167 (2000).
 [5] J. Bergenholtz, J. F. Brady, and M. Vicol, *J. Fluid Mech.* **456**, 239 (2002).
 [6] X. Cheng, J. H. McCoy, J. N. Israelachvili, and I. Cohen, *Science* **333**, 1276 (2011).
 [7] B. M. Guy, M. Hermes, and W. C. K. Poon, *Phys. Rev. Lett.* **115**, 088304 (2015).
 [8] C. D. Cwalina and N. J. Wagner, *J. Rheol.* **58**, 949 (2014).
 [9] C. G. de Kruif, E. M. F. van Iersel, A. Vrij, and W. B. Russel, *J. Chem. Phys.* **83**, 4717 (1985).
 [10] W. C. K. Poon, E. R. Weeks, and C. P. Royall, *Soft Matter* **8**, 21 (2012).
 [11] S.-E. Phan, W. B. Russel, Z. Cheng, J. Zhu, P. M. Chaikin, J. H. Dunsmuir, and R. H. Ottewill, *Phys. Rev. E* **54**, 6633 (1996).
 [12] W. B. Russel, N. J. Wagner, and J. Mewis, *J. Rheol.* **57**, 1555 (2013).
 [13] Y. S. Papir and I. M. Krieger, *J. Colloid Interface Sci.* **34**, 126 (1970).
 [14] M. E. Woods and I. M. Krieger, *J. Colloid Interface Sci.* **34**, 91 (1970).
 [15] J. C. van der Werff and C. G. de Kruif, *J. Rheol.* **33**, 421 (1989).
 [16] Certain instruments and materials are identified in this paper to adequately specify the experimental details. Such identification does not imply recommendation by the National Institute of Standards and Technology nor does it imply the materials are necessarily the best available for the purpose.
 [17] H. M. Laun, *J. Non-Newton. Fluid* **54**, 87 (1994).
 [18] M. Lee, M. Alcoutlabi, J. J. Magda, C. Dibble, M. J. Solomon, X. Shi, and G. B. McKenna, *J. Rheol.* **50**, 293 (2006).
 [19] A. K. Gurnon and N. J. Wagner, *J. Fluid Mech.* **769**, 242 (2015).
 [20] I. E. Zarraga, D. A. Hill, and D. T. Leighton, *J. Rheol.* **44**, 185 (2000).
 [21] A. Singh and P. R. Nott, *J. Fluid Mech.* **490**, 293 (2003).
 [22] S.-C. Dai, E. Bertevras, F. Qi, and R. I. Tanner, *J. Rheol.* **57**, 493 (2013).
 [23] T. Dbouk, L. Lobry, and E. Lemaire, *J. Fluid Mech.* **715**, 239 (2013).
 [24] C. Gamonpilas, J. F. Morris, and M. M. Denn, *J. Rheol.* **60**, 289 (2016).
 [25] C. R. Schultheisz and S. D. Leigh, in *NIST special publication 260-143* (U.S. Dept. of Commerce, Tech. Admin., NIST, 2001).